Journal of Power Sources 195 (2010) 5719–5725

Contents lists available at ScienceDirect

Journal of Power Sources

journal homepage: www.elsevier.com/locate/jpowsour

Performance of tubular Solid Oxide Fuel Cell at reduced temperature and cathode porosity

Ahmad K. Sleiti

The William States Lee College of Engineering, UNC Charlotte, 9201 University City Blvd., Charlotte, NC 28223, United States

ARTICLE INFO

Article history:
Received 22 January 2010
Received in revised form 12 March 2010
Accepted 12 March 2010
Available online 20 March 2010

Keywords:
Solid Oxide Fuel Cell
Cathode porosity
Modeling tubular SOFC

ABSTRACT

The effect of decreasing the inlet temperature and the cathode porosity of tubular Solid Oxide Fuel Cell (SOFC) with one air channel and one fuel channel is investigated using Computational Fluid Dynamics (CFD) approach. The CFD model was developed using Fluent SOFC to simulate the electrochemical effects. The cathode and the anode of the cell were resolved in the model and the convection and conduction heat transfer modes were included. The results of the CFD model are presented at inlet temperatures of 700 °C, 600 °C and 500 °C and with cathode porosity of 30%, 20% and 10%. It was found that the Fluent-based SOFC model is an effective tool for analyzing the complex and highly interactive three-dimensional electrical, thermal, and fluid flow fields associated with the SOFCs. It is found that the SOFC can operate in the intermediate temperature range and with low porosity cathodes more efficient than at high temperatures given that the transport properties of the cathode, anode and the electrolyte can be kept the same.

1. Introduction

With the capability to generate electricity efficiently between 1 kW and 1 MW with little or no toxic emissions, fuel cells in general, and Solid Oxide Fuel Cells (SOFCs) in particular, are poised to have a significant impact in the distributed power generation sector worldwide. The suitability of SOFC technology for combined heat and power generation applications along with the potential for high efficiency systems when used in tandem with a gas turbine are well recognized. While the development of innovative cell designs to enhance electrical performance is a necessary step, a key element in the pursuit for commercialization is also the operation and thermal management within a stack environment. Isothermal cell tests and button cell tests, due to their relative simplicity, have been used traditionally to characterize the electrical performance of the SOFCs and evaluate thermal cycling. However, the thermal and flow fields within a stack generally result in non-isothermal conditions, which not only affect the cell performance, but can also induce deleterious thermal and mechanical stresses in the cells that can lead ultimately to a failure. Experimental evaluation of the performance under stack operating conditions using prototypical stack tests is expensive and requires significant turn-around time. It is also difficult to isolate the effects of one particular parameter. Consequently, computational models are invaluable in extending the measured isothermal cell characteristics and fundamental mechanical properties to predict both electrical performance and mechanical behavior of SOFCs in a stack under different operating conditions.

A current problem with SOFCs is their relatively high operating temperatures, which are required for obtaining high output voltage potentials, high power densities, and high efficiencies. This operating temperature, usually around 800–1000 °C, not only limits where SOFCs can be presently used, but also makes them costly, needing more exotic interconnect and housing components that can handle such temperatures. At these high temperatures, electrode sintering, interfacial diffusion between the electrodes and the electrolyte, and mechanical stresses due to thermal incompatibility are of great concern [1]. Thermal expansion compatibility issues between the electrodes and the electrolyte are a major problem, leading to hours-long start up and shut down times in order to go either direction from the operating temperature to an ambient temperature [2].

In the present study, the aim is to lower the operating temperature to an intermediate temperature range, which is considered to be approximately 500–800 °C, while still obtaining high power densities from a SOFC by parametric evaluation of transport phenomena in a three-dimensional SOFC model. This evaluation will allow for the determination of the most critical processes and associated parameters for SOFC performance and optimal material parameters and operating conditions maybe determined for future research and manufacturing. In lowering the SOFC operational temperature to an intermediate range, significantly cheaper sealing technologies and inexpensive interconnect components can be utilized, drastically reducing the overall energy cost [2]. An oper-

E-mail address: asleiti@uncc.edu.

0378-7753/$ – see front matter © 2010 Elsevier B.V. All rights reserved.
doi:10.1016/j.jpowsour.2010.03.044

Nomenclature

a	the stoichiometric coefficient
CFD	Computational Fluid Dynamics
D_{ij}	binary diffusivity of a species i into species j ($m^2\ s^{-1}$)
F	Faraday constant (965×10^7 C kg mol^{-1})
FU	fuel utilization
i	the local current density (A)
IC	interconnect
J	current density (A m^{-2})
n	the number of electrons per mole of fuel
S	the source or sink of the species
SOFC	Solid Oxide Fuel Cell
t	thickness (m)
T_{in}	oxygen and hydrogen inlet temperature (K)
U	utilization
UDF	user defined function
V–J	voltage–current density variation

Greek letters

ε	the porosity and (%)
τ	the tortousity
σ	the electrical conductivity ($1\ \Omega^{-1}\ m^{-1}$)
ϕ	the electrical potential (V)
η	overpotential (V)

able SOFC system in this intermediate temperature range, known as an intermediate temperature SOFC or ITSOFC, will allow for greater application and cheaper manufacturability, which are goals necessary for competitive use of SOFCs in future energy systems.

The electrode microstructure involves the meso-scale properties of surface area, triple phase boundary (TPB) length, volume fraction of chemical phases present, tortuosity of fuel/air flow and electron transport [3,4]. These properties involve the reaction kinetics, charge transport, and mass transport processes that govern the performance of a fuel cell. The main electrode of focus is the cathode, since it is the location of the kinetically slow O_2 reduction reaction. The losses associated with the cathode reaction kinetics are the greatest detriment to ITSOFC power output relative to high temperature performance.

The active surface area of the reactions occurring in a fuel cell relates to the triple phase boundary (TPB) length, defined as the area where the electrode surface, electrolyte surface, and reactant or product gas phase meet. This is the only area in the fuel cell where the electrochemical reactions that involve a voltage response occur. The reaction at the cathode TPB, which is the oxygen reduction reaction, is the most critical to SOFC performance due to the sluggish reaction rate relative to the hydrogen oxidation reaction at the anode TPB. To combat the slow oxygen reduction reaction kinetics, mixed ionic and electronic conducting, or MIEC, composite cathodes are utilized to lengthen this reaction area [2]. If this active length is increased, more electrochemical reactions can take place, and a higher voltage output can be created from a cell. The limit to active sites comes from physical constraints and material strength and integrity [4]. In order to create more active sites porosity and tortuosity, as well as the localized TPB pore and grain sizes, of the cathode material are considered. Porosity is defined as the ratio of pore volume to total volume, meaning how much volume is occupied in the form of open space, or pores, in a percentage form [4,5]. An increase in porosity at the electrode/electrolyte interface leads to less diffusion resistance and more effective TPB length, increasing the active sites and overall fuel cell performance. Tortuosity, a related electrode microstructure property, is a measure of a bulk diffusion resistance, relating how well gases can penetrate through a material, which, in fuel cells, is the thickness of an electrode [5,4]. Tortuosity may also be used as a parameter encompassing everything unknown about a material microstructure, almost like an experimentally calibrated value [5]. Tortuosity is mainly related to the diffusion processes of mass transport in a fuel cell. A lower tortuosity value indicates a shorter path for the reactant (or product) to travel through the electrode layer, increasing reactant at the TPB sites; therefore, increasing cell performance. Both tortuosity and porosity are defining components of electrode microstructure that maybe manipulated for better fuel cell performance, as is performed in a modeling study.

Many SOFC models have trouble accurately portraying fuel cell performance at such tortuosities when compared with experimental data [6]. The models typically function correctly only with tortuosities in the range of 10–17 [6]. In these cases, more complex issues with the mass transport processes in the electrode microstructure must be considered, such as non-ideal gas behavior, Knudsen effects, competitive adsorption, and surface diffusion [4]. In the current study the cathode porosity effect will be investigated. Both the porosity and the tortuosity have been related to the concentration overpotential, however, they also play an important role in the activation overpotential.

The main objective of the present investigation is to study the effect of reducing the cell temperature and the cathode porosity on the cell performance. The ultimate future objective is the development of a multi-scale multi-physics model to capture the transport processes at macro, micro and nanoscales for newly developed low porosity cathodes with elevated electrochemical performance. A CFD model of a tubular SOFC cell is used based on the commercial CFD software Fluent 6.2 (Fluent, Inc.). Thermal and flow field results obtained with the model are presented and discussed. The comprehensive current density and thermal fields generated with the CFD model are necessary to assist a life-cycle analysis of the cell through prediction of thermal stresses.

2. CFD modeling

CFD modeling of fuel cells is achieved by numerically solving the governing set of fundamental partial differential equations that describe the fluid flow, heat and mass transfer, and the chemical and electrochemical reactions that occur in fuel cells. The numerical solution can provide spatial distributions of the fluid velocity, temperature, pressure, chemical species, electric current, fuel consumption, water formation, power density, etc. The three-dimensional complex phenomena of the fluid flow, heat transfer, and chemical and electrochemical reactions in fuel cells require multidimensional modeling approach for SOFC (Autissier et al. [7]). Commercial CFD codes, such as FLUENT, CFX, STAR_CD, and FEMLAB, have shown noticeable progress. However, complete and fully validated modeling methodology that can accurately model the various complex processes in the fuel cells is yet to be established, especially for the modeling of stacks and unsteady fuel cell operating conditions (see Beale et al. [8]).

There have been several comprehensive numerical simulations of electrical and thermal performance of SOFCs. Bessette et al. [9], Nagata et al. [10], Li and Chyu [11], and Campanari and Iora [12] have analyzed tubular SOFCs, while Achenbach [13], Yakabe et al. [14], and Recknagle et al. [15] have focused their investigations on planar SOFCs. Ferguson et al. [16] included both the tubular and the planar SOFCs in their studies. Lu et al. [17] have investigated flattened tube high power density cell geometry. Nevertheless a majority of the numerical models have been developed based on finite difference, finite volume or finite element techniques for the specific situation analyzed with some flexibility for the perturbations of geometrical dimensions about the basic shape. Radiative

heat exchange, a significant energy transfer mechanism in high temperature SOFC [18–20] has been either neglected or simplified in many of these models.

The use of commercial CFD codes to develop the geometric model and to solve the transport equations along with user defined functions for modeling electrochemistry was considered for this work. Other SOFC modules have already been developed for several commercial codes including, Fluent (Fluent, Inc.), MARC (MSC Software), CFD-ACE+ (ESI group), and STAR-CD (CD-adapco).

- In Khaleel et al. [21] the MARC SOFC interface and the electrochemical routine is described, which includes structural analysis capability.
- At the U.S. Pacific Northwest National Laboratory Khaleel et al. [21] have also integrated their electrochemical model into the commercial code STAR-CD (see [16] for example).
- Reich et al. [22] showed the electrochemical capability in CFD-ACE+.
- The electrochemical user defined function (UDF) for Fluent was developed by the U.S. National Energy Technological Laboratory (NETL) and is described in Rogers et al. [23].

Fluent CFD code is implemented for the current simulation due to its generalized formulation of the electrochemical model that could be applied to any cell geometry.

2.1. SOFC model description

The Fluent SOFC UDF is described in detail in [23,24]. In essence, it is composed of an electrochemical submodel, an electrical submodel, and a porous media mass diffusion model. The electrochemical model evaluates the Nernst potential, the cathode and anode activation polarizations, at the electrolyte, which is modeled as a thin wall. A Butler–Volmer formulation is used to model electrode kinetics and the activation losses. The respective rate of depletion and generation of the reactants and the products of the electrochemical reaction are computed based on the local current density. The electrochemical reaction is modeled by placing mass sources and sinks for the reactants and products, respectively, that correspond to the computed rates in the anode and cathode regions immediately neighboring the electrolyte. To ensure accurate energy balance, the net energy released at the electrolyte is computed by a local enthalpy balance at the electrolyte and is split between the cathode and the anode sides.

The electrical field submodel solves for the electrical potential field in the conductive layers of the cell, using Fluent's capability to solve a conservation equation for a user defined scalar. A potential jump at the electrolyte, corresponding to the difference between the local Nernst potential and the sum of electrode activation losses, is used to connect the air electrode and fuel electrode potential fields. The production of heat due to Ohmic heating throughout the electrical field is computed from the current density field. Both the air electrode and the fuel electrode are modeled as porous media. The mass diffusion model corrects for diffusion in the porous media through tortuosity and porosity values and models concentration polarizations directly using the multi-component diffusion models in Fluent.

The electrical field submodel and the mass diffusion model are particularly of interest for cell geometries where the electrical and species diffusion fields are too intricate to be represented by lumped resistance networks. The electrical conductivity of the air electrode (AE), the fuel electrode (FE), the electrolyte, and the interconnection (IC), and the exchange current densities of the electrodes are amongst the list of parameters that are used to define the cell electrochemistry. A complete list of parameters used to define the electrochemical model can be found in [23,24] and a summary of the model outline is provided below [24] for the convenience of the readers.

2.1.1. Outline of the SOFC model

In the electrochemical model, the two sides of the electrolyte are separated by a local potential difference. This difference is determined by Nernst potential, Ohmic losses in the electrolyte, and activation losses at the electrode–electrolyte interfaces.

$$\delta V = N - i\rho_{\text{ele}} t_{\text{ele}} - \eta_{\text{act}}(i) \tag{1}$$

where i is the local current density.

All aspects of fluid flow, heat transfer, and mass transfer in the flow channels and porous electrodes are handled by the model. The multi-component diffusion model is used to calculate the mass diffusion coefficient of species i in the mixture. To account for the effect of porosity on the multi-component mass diffusion coefficient

$$D_{ij,\text{eff}} = \frac{\varepsilon}{\tau} D_{ij} \tag{2}$$

where ε is the porosity and τ is the tortousity.

The potential field throughout the conductive regions is calculated based on the conservation of charge.

$$\nabla\ i = 0 \tag{3}$$

where i is

$$i = -\sigma \nabla \phi \tag{4}$$

and σ is the electrical conductivity and ϕ is the electrical potential. Therefore, the governing equation for the electric field is the Laplace equation:

$$\nabla(\sigma \nabla \phi) = 0 \tag{5}$$

The activation overpotential is treated by building a linearized form of the Butler–Volmer relation:

$$\eta_{\text{act}}(i) \approx \eta_{\text{o}} - \eta_1 (i - i_{\text{old}}), \quad \eta_{\text{o}} = \eta_{\text{act}}(i_{\text{old}}), \quad \eta_1 = -\left.\frac{\partial \eta_{\text{act}}}{\partial i}\right|_{i=i_{\text{old}}} \tag{6}$$

The relation for the voltage jump across the electrolyte then becomes:

$$V \approx [N - \eta_{\text{o}} + \eta_1 i_{\text{old}}] - i[\rho_{\text{ele}} t_{\text{ele}} + \eta_1] \tag{7}$$

The electric field and the electrochemistry interact solely at the electrolyte interface. FLUENT treats the electrolyte interface as an impermeable wall. The potential field must have a jump condition applied to the two sides of this wall to account for the effect of the electrochemistry. To closely couple the electrochemical behavior to the potential field calculation, you need to include all of the electrochemical effects into this jump condition. It encapsulates the voltage jump due to Nernst, the voltage reduction due to activation, the Ohmic losses due to the resistivity of the electrolyte, and a linearized for voltage reduction due to activation. This interface condition relates the potential on the anode side and the cathode side of the electrolyte and has the following form:

$$\phi_{\text{cell}} = \phi_{\text{jump}} - \eta_s \tag{8}$$

where

$$\phi_{\text{jump}} = \phi_{\text{ideal}} - \eta_{\text{ele}} - \eta_{\text{act,a}} - \eta_{\text{act,c}} \tag{9}$$

where η_{ele} represents the Ohmic overpotential of the electrolyte, and $\eta_{\text{act,a}}$ and $\eta_{\text{act,c}}$ represent the activation overpotential of the anode and the cathode. η_s represents the Ohmic losses in the solid conducting regions. ϕ_{ideal} represents the Nernst potential.

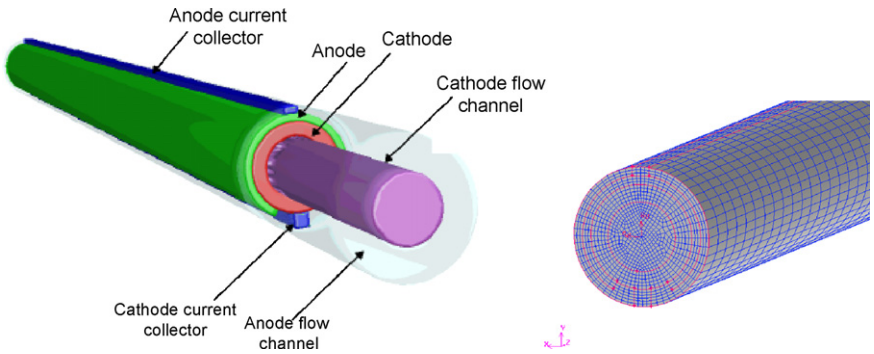

Fig. 1. Geometry and numerical grid.

The model solves the Laplace equation for the potential field by subdividing the computational domain into control volumes and enforcing flux conservation on each cell.

Ohmic polarization involves ionic losses through the electrolyte, electrical resistance in the conducting porous electrodes and solid collectors and includes the electrical resistance at the interface of the current collectors and the electrodes:

$$\eta_{\text{ohmic}} = i\ R \tag{10}$$

The activation overpotential at the anode ($\eta_{\text{act,a}}$) and the cathode ($\eta_{\text{act,c}}$) can be determined based on the Butler–Volmer equation:

$$\eta_{\text{act}} = \frac{2RT}{nF} \sinh^{-1}\left(\frac{i}{2i_{0\text{eff}}}\right) \tag{11}$$

The rate of species production and destruction is:

$$S(\text{g mole/s}) = -\frac{ai}{nF} \tag{12}$$

where S is the source or sink of the species, a is the stoichiometric coefficient, i is the current, n is the number of electrons per mole of fuel, and F is the Faraday constant. Using the local current information, the SOFC model applies species fluxes to the electrode boundaries. Hence, the reactions at the cathode and anode electrodes are:

$$S_{\text{O}}^{2-} = -\frac{(-i)}{2F} = -\frac{i}{2F}, \quad S_{\text{H}_2\text{O}} = -\frac{-(1)(i)}{2F} = \frac{i}{2F} \tag{13}$$

2.2. Cell geometry, CFD domain, and computational grid

The tubular SOFC with one air channel and one fuel channel is shown schematically in Fig. 1. A CFD model of the cell was developed using Fluent's pre-processor Gambit 2.2.3 (Fluent, Inc.), and is shown in Fig. 1. The anode inlet is fed with 2.48949e−07 kg s^{-1} of humidified hydrogen (80% H_2 and 20% H_2O) at 973 K and 1 atm. The cathode inlet is fed with 1.3705e−05 kg s^{-1} of air at 973 K and 1 atm. The cathode and anode comprise two concentric cylinders, each 130 mm long. The inner and outer diameters of the cathode are 4 mm and 6 mm, respectively. The inner and outer diameters of the anode are 6 mm and 7 mm, respectively.

The active electrolyte material, which has a thickness of 40 μm, is pressed between the anode and the cathode layers. In this simulation, the outer walls of the anode and cathode current collectors are kept insulated. The fuel and oxidizer travel through the porous anode and cathode materials toward the electrolyte region. Fuel is oxidized electrochemically at the interface of the electrolyte region and the anode. Oxygen in the incoming air is reduced electrochemically at the interface of the electrolyte region and the cathode. As a result of the overall reaction, water is formed at the anode side. The SOFC model is used to examine the current, voltage, species, and temperature distribution throughout the fuel cell.

The cathode, anode and current collector were all included in the model. The electrolyte was modeled using a thin wall approximation. The Fluent UDF requires a voltage tap and a current collector, which set the boundary conditions for the electrical potential field. A busbar along with a powerlead shown in Fig. 1 represent the current collectors. The option of using periodic boundary conditions for the electrical potential field is not available currently. Hence, the cell modeled in Fig. 1 is more representative of a peripheral cell in the generator. The final computational mesh is shown in Fig. 1 and consists of about 79,680 finite volume computational cells. The Fluent steady segregated incompressible solver was used in these calculations. The air and the fuel flows are both laminar.

3. Results and discussion

3.1. Model validation

To validate the simulation results from this study a comparison with the experimental data of Hagiwara et al. [25] was performed. In this simulation, the values of fuel and air flow rates were adjusted to match the values of utilization factors given in [25]. For different operating cell potentials, they were found to vary from 0.002 kg h^{-1} to 0.008 kg h^{-1} for the fuel and 0.4 kg h^{-1} to 0.9 kg h^{-1} for air. The current–potential results shown in Fig. 2 are in good agreement with experimental data to within less than 5% for current densities between 1100 A m^{-2} and 3900 A m^{-2}. However, the agreement is within 10% outside that range. This behavior maybe attributed to the difference in the perfect conditions of the simulation compared to the actual experimental conditions that usually has several sources of uncertainty.

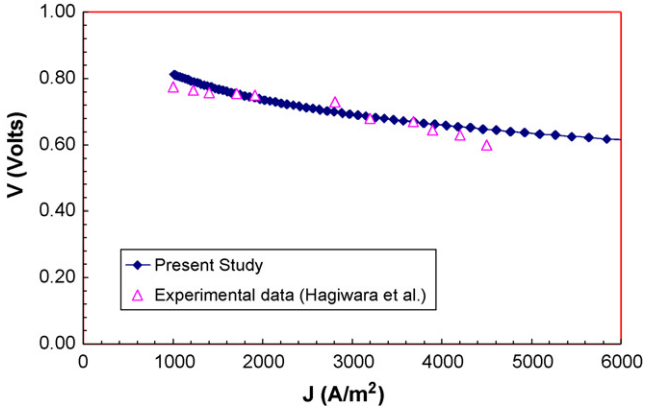

Fig. 2. Comparison of current–potential from the present study with experimental data from Hagiwara et al. [25] at $U_{\text{air}} = 0.167$ and $U_{\text{fuel}} = 0.85$.

Table 1
SOFC model input parameters.

Parameter	Value
Total system current	9 A
Electrolyte thickness	0.000175 m
Electrolyte resistivity	0.2 W m
Anode exchange current density	1e+20 A
Cathode exchange current density	1000 A
Anode H_2 mole fraction reference	1 mole mole^{-1}
Anode H_2O mole fraction reference	1 mole mole^{-1}
O_2 mole fraction reference	1 mole mole^{-1}
Anode conductivity	333,330 (1 Ω^{-1} m^{-1})
Cathode conductivity	7937 (1 Ω^{-1} m^{-1})
Anode contact resistance	1e−08 (Ω m^2)
Cathode contact resistance	1e−07 (Ω m^2)
Anode tortuosity parameters	3
Cathode tortuosity parameters	3

3.2. Simulation results

Since there are many different processes and parameters in SOFC operation, it is important to determine which processes are the most detrimental to SOFC performance in the intermediate temperature range. In the simulation model, each of the major losses, activation, Ohmic, and concentration, were calculated separately, using the appropriate equations, and were analyzed at different temperatures and porosities. The values used in this simulation for the electrical, electrochemical and activation parameters are given in Table 1.

Fig. 3 shows contours of the current density Nernst voltage and temperature distribution on the electrolyte wall. Both current density and Nernst voltage are decreasing from the inlet to the exit. It is noticed that the temperature of the electrolyte is increasing rapidly from the inlet to the exit. The high temperatures and the low current density values near the exit indicate that the cell length needs to be reduced to achieve an optimized design.

The voltage increases by decreasing temperature from 973 K to 873 K and 773 K as shown in Figs. 4 and 5. Notice that the voltage and current density values shown in Figs. 3 and 4 represent the values distribution from the cell inlet to the exit. The voltage increases by decreasing porosity of the cathode from 30% to 20%, while decreasing the porosity from 20% to 10% has no effect on the voltage as shown in Fig. 3 where the two curves lie on top of each other. Surprisingly, the highest voltage is achieved at 773 K and 30% porosity. This implies that it is possible to operate the SOFC fuel at low temperatures and cathode porosities given that the properties of the SOFC components can be kept the same.

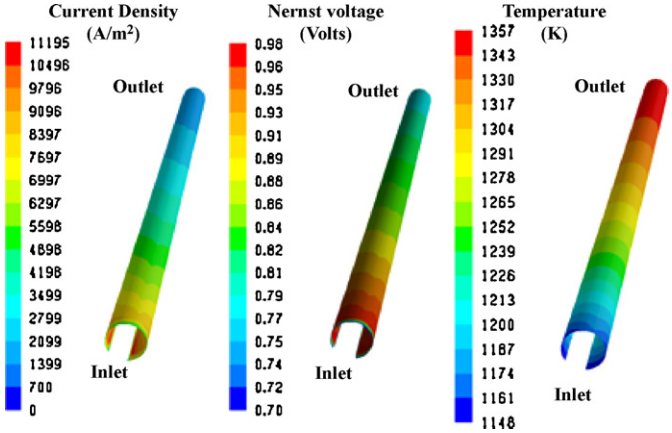

Fig. 3. Contours of current density in A m^{-2}, Nernst voltage in V and temperature distribution in K on the electrolyte (T_{in} = 973 K, 30% cathode porosity).

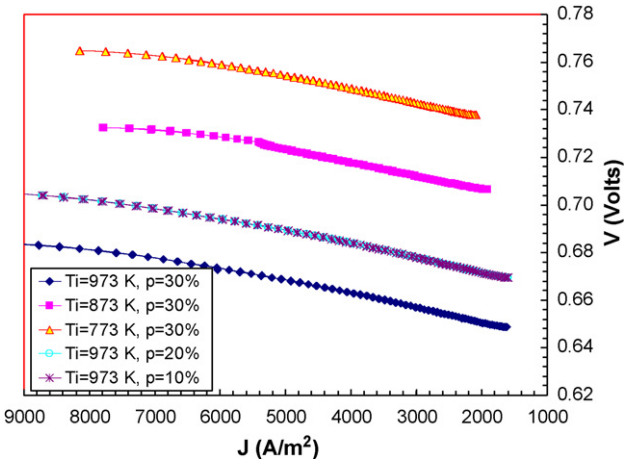

Fig. 4. Current density vs voltage, effect of reducing temperature and porosity.

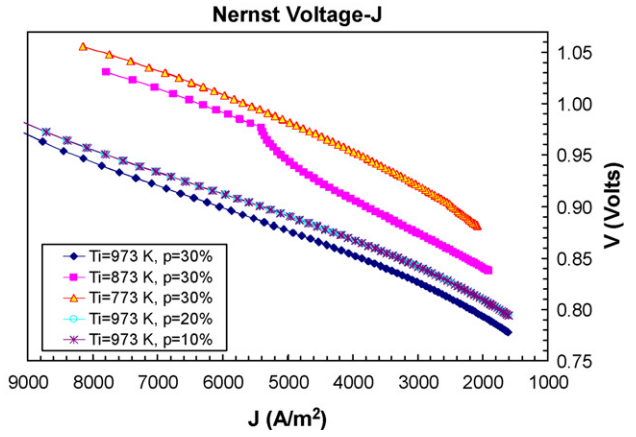

Fig. 5. Current density vs Nernst voltage, effect of reducing temperature and porosity.

The electrolyte temperature decreases by decreasing the inlet temperature of the air and the fuel as shown in Fig. 6. The temperature also decreases by decreasing the porosity from 30% to 20% which is consistent with the increase in voltage. Decreasing the porosity from 20% to 10% has no effect on temperature. The lowest temperature is achieved for the case of T_{in} = 773 K and 30% porosity. Fig. 6 also shows that the electrolyte temperature increases from the inlet to exit of the cell from 773 K to about 1080 K (more than

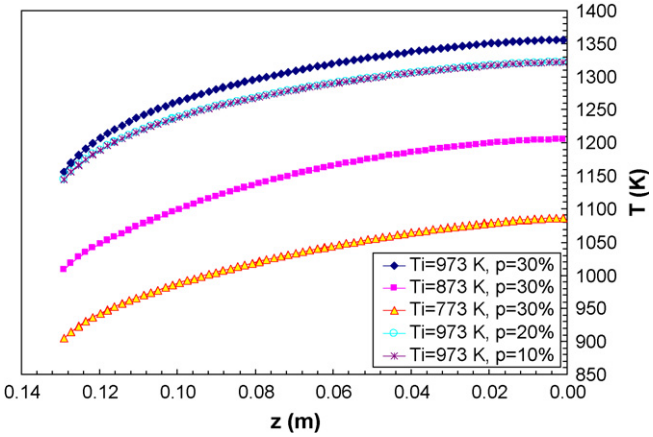

Fig. 6. Electrolyte temperature along the cell, effect of reducing temperature and porosity.

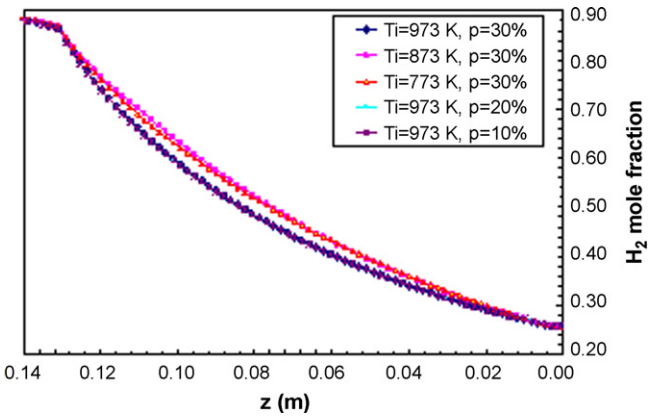

Fig. 7. H_2 mole fraction along the cell fuel channel, effect of reducing temperature and porosity.

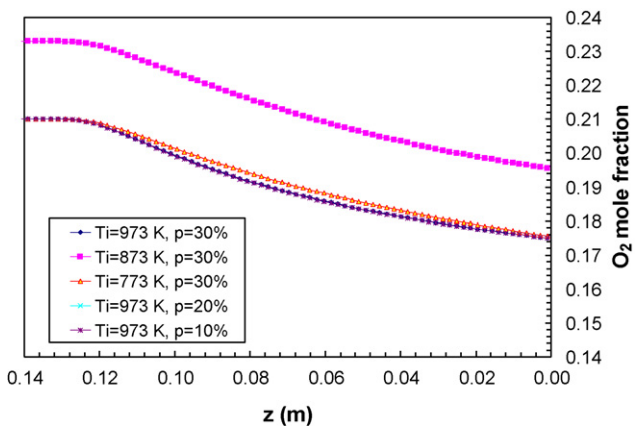

Fig. 9. O_2 mole fraction along the cell fuel channel, effect of reducing temperature and porosity.

300 K), which is a significant increase that can be reduced using less porous cathodes with better transport properties.

Fig. 7 shows that decreasing temperature from 973 K to 873 K at the same cathode porosity of 30% caused a slight decrease in H_2 mole fraction starting from the inlet of the cell to the exit. Decreasing the temperature further to 773 K did not affect H_2 mole fraction any further. Decreasing the porosity has no effect on the H_2 mole fraction.

Results shown in Fig. 8 suggest that decreasing temperature from 973 K to 873 K at the same porosity of 30% caused a decrease in H_2O mole fraction starting from the inlet of the cell to the exit, which is consistent with H_2 mole fraction behavior. Decreasing the temperature further to 773 K has not effect on the H_2O mole fraction any further. Decreasing the porosity has no effect on the H_2O mole fraction.

Decreasing temperature from 973 K to 873 K at the same porosity of 30% caused an increase in O_2 mole fraction starting from the inlet of the cell all the way to the exit as shown in Fig. 9. Decreasing the temperature further to 773 K caused a decrease in the mole fraction to similar levels as for the case of 973 K. This finding is not completely understood and needs further exploration in the future. However, this suggests that by operating the fuel cell at low temperatures of about 773 K the O_2 mole fraction levels can be kept the same as at higher temperatures of about 973 K. Decreasing the porosity at the same temperature has no effect on the O_2 mole fraction.

The activation overpotential as shown in Fig. 10 decreases by decreasing temperature from 973 K to 873 K and 773 K. The activation overpotential decreases by decreasing porosity of the cathode from 30% to 20%, while decreasing the porosity to 10% has no effect on the activation overpotential. The lowest activation overpotential is found at 773 K and 30% porosity. The reduced activation overpotential depicted in Fig. 10 explains the improved cell voltages mentioned earlier. This implies that the design of the fuel cell can be enhanced significantly and the fuel cell can operate at intermediate temperatures while elevating the performance to even higher levels than operating at high temperatures given that all other properties of the fuel cell components can be kept the same.

3.3. Materials for ITSOFC

In order to develop materials for the ITSOFC with the desired properties, two commercial 10 mol% Sc_2O_3–1 mol% CeO_2–ZrO_2 powders manufactured by Praxair Surface Technologies, Specialty Ceramics, USA and DKKK, Japan were compared for use as an electrolyte material for Intermediate Temperature SOFCs. Single element SOFCs were developed using $ScCeZrO_2$ dense ceramics as an electrolyte, composite 50 wt% $La_{0.6}Sr_{0.4}Fe_{0.8}Co_{0.2}O_3$ (LSFC) + 50 wt% Gd_2O_3 + CeO_2 (GDC) porous ceramics as a cathode, and Ni–$ScCeZrO_2$ cermet as an anode. It is found that the $ScCeZrO_2$ DKKK powder densifies more easily than that of Praxair powder. It is also found that the optimal sintering temperature for 50 wt% LSFC–50 wt% GDC cathode powders is 1100–1200 °C, but that sintering begins as low as 800 °C. The optimal sintering temperature for the 50 wt% DKKK $ScCeZrO_2$–50 wt% NiO anode powder is between 1050 °C and 1100 °C. The electrolyte tapes have been produced by the tape casting followed by sintering at 1500 °C for 2 h. Then, the anode and cathode has been screen printed on both sides of the electrolyte layer. Completed button cells containing the

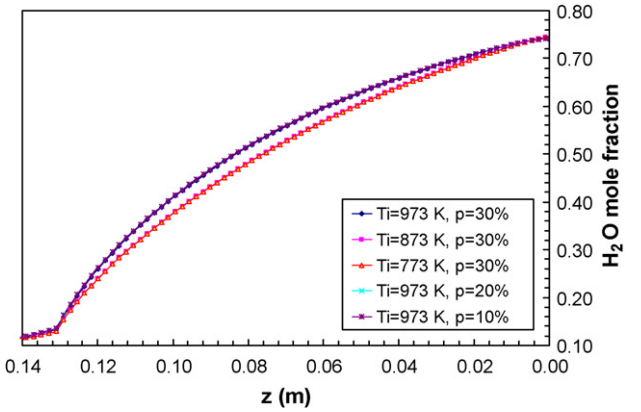

Fig. 8. H_2O mole fraction along the cell fuel channel, effect of reducing temperature and porosity.

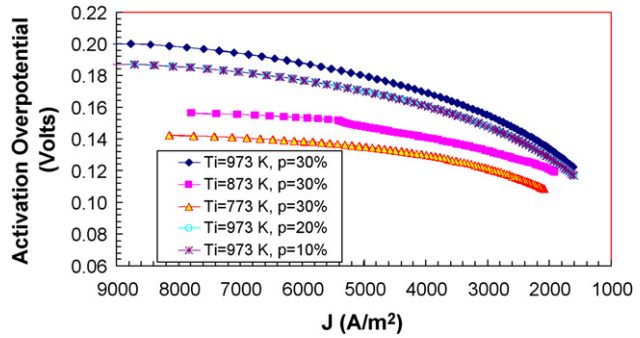

Fig. 10. Activation overpotential vs current density, effect of reducing temperature and porosity.

screen printed anode and cathode were sintered in air at 1100 °C for 2 h. Button cells were tested at 800 °C using a 97% H_2 and 3% H_2O on the anode side and air on the cathode side.

The first preliminary results showed the cell performance of only 28 mW cm^{-2} maximum power density achieved at 0.74 V. This limited performance maybe attributed to the sintering of the electrodes during testing and the formation of poorly conducting secondary phases at one of the electrode/electrolyte interfaces.

More studies on developing ITSOFC materials with elevated properties are ongoing and will be reported in future work side by side with modeling studies.

4. Conclusions

The effect of decreasing the inlet temperature to intermediate levels of about 773 K and decreasing the cathode porosity of tubular Solid Oxide Fuel Cell with one air channel and one fuel channel is studied using CFD approach. A Fluent-based SOFC model was used to simulate the electrochemical effects. The cathode and the anode of the cell were resolved in the model and the convection and conduction heat transfer modes were included. The results of the CFD model are presented at inlet temperatures of 973 K, 873 K, and 773 K, with cathode porosity of 30%, 20% and 10%. The resulting thermal, electrical, and flow fields showed that the fuel cell voltage increases by decreasing temperature from 973 K to 873 K and 773 K. The voltage increases by decreasing porosity of the cathode from 30% to 20%, while decreasing the porosity to 10% has no effect on the voltage. The highest voltage is achieved at 773 K and 30% porosity. This implies that the SOFC can operate in the intermediate temperature range and with low porosity cathodes more efficiently than at high temperatures given that the transport properties of the cathode, anode and the electrolyte can be kept the same. Furthermore, this conclusion implies that there is a potential that some of the fragile ceramic components of the SOFC can be replaced with more reliable metal components.

References

[1] B. Huang, X. Ye, S. Wang, H. Nie, R. Liu, T. Wen, Materials Research Bulletin 42 (2007) 1705–1714.
[2] S. Baron, Intermediate Temperature (500–850 °C) Solid Oxide Fuel Cells (IT-SOFCs) Explained [Online Document], 2004 [2009 Jan], Available at http://www.fuelcelltoday.com.
[3] W. Huang, X. Huang, K. Reifsnider, Proceedings of the COMSOL Users Conference, Boston, MA, 2006.
[4] R. O'Hayre, S. Cha, W. Colella, F. Prinz, Fuel Cell Fundamentals, John Wiley & Sons, Inc., New York, 2006.
[5] L. Chick, R. Williford, J. Stevenson, C. Windisch, ASME Conference, Fuel Cell Seminar, San Diego, CA, 2002.
[6] R. Williford, L. Chick, G. Maupin, S. Simner, S. Stevenson, Journal of the Electrochemical Society 150 (8) (2003).
[7] N. Autissier, D. Larrain, J. Van herle, D. Favrat, Journal of Power Sources 131 (2004) 313–319.
[8] S.B. Beale, Y. Lin, S.V. Zhubrin, W. Dong, Journal of Power Sources 118 (2003) 79–85.
[9] N.F. Bessette II, W.J. Wepfer, J. Winnick, Journal of the Electrochemical Society 142 (11) (1995) 3792–3800.
[10] S. Nagata, A. Momma, T. Kato, Y. Kasuga, Journal of Power Sources 101 (2001) 60–71.
[11] P. Li, M.K. Chyu, Journal of Power Sources 124 (2003) 487–498.
[12] S. Campanari, P. Iora, Journal of Power Sources 132 (2004) 113–126.
[13] E. Achenbach, Journal of Power Sources 49 (1994) 333–348.
[14] H. Yakabe, T. Ogiwara, M. Hishinuma, I. Yasuda, Journal of Power Sources 102 (2001) 144–154.
[15] K.P. Recknagle, R.E. Williford, L.A. Chick, D.R. Rector, M.A. Khaleel, Journal of Power Sources 113 (2003) 109–114.
[16] J.R. Ferguson, J.M. Fiard, R. Herbin, Journal of Power Sources 58 (1996) 109–122.
[17] Y. Lu, L. Schaefer, P. Li, Journal of Power Sources 140 (2005) 331–339.
[18] D.L. Damm, A.G. Fedorov, Journal of Power Sources 143 (2005) 158–165.
[19] S. Murthy, A.G. Fedorov, Journal of Power Sources 124 (2003) 453–458.
[20] J.D.J. VanderSteen, Pharoah, The Effect of Radiation Heat Transfer in Solid Oxide Fuel Cell Modeling, Combustion Institute/Canadian Section, Spring Technical Meeting, Queen's University, 2004.
[21] M.A. Khaleel, Z. Lin, P. Singh, W. Surdoval, D. Collin, Journal of Power Sources 130 (2004) 136–148.
[22] A.J. Reich, R. Das, J.V. Cole, S. Mazumder, Fourth International ASME/KSME/JSME Symposium on Computational Technologies for Fluid/Thermal/Chemical Systems with Industrial Applications, August 4–8, 2002, Vancouver, BC, Canada, 2002.
[23] W.A. Rogers, R.S. Gemmen, C. Johnson, M.T. Prinkey, M. Shahnam, Proceedings of the First International Conference on Fuel Cell Science Engineering and Technology, Rochester, NY, April 21–23, 2003.
[24] M.T. Prinkey, M.S. Shahnam, W.A. Rogers, SOFC FLUENT Model Theory Guide and User Manual, Fluent UDF Manual, 2003.
[25] A. Hagiwara, H. Michibata, A. Kimura, M.P. Jaszcar, G.W. Tomlins, S.E. Veyo, Proceedings of the Third International Fuel Cell Conference, D2-4, 1999, p. 369.